In-Situ Measurements of Engineered Nanoporous Particle Transport in Saturated Porous Media

ARTICLE *in* ENVIRONMENTAL SCIENCE & TECHNOLOGY · OCTOBER 2010

Impact Factor: 5.33 · DOI: 10.1021/es1015586 · Source: PubMed

7 AUTHORS, INCLUDING:

Jianying Shang
Pacific Northwest National Laboratory
20 PUBLICATIONS **298** CITATIONS
SEE PROFILE

Chongxuan Liu
Battelle Memorial Institute
147 PUBLICATIONS **3,938** CITATIONS
SEE PROFILE

Zheming Wang
Pacific Northwest National Laboratory
181 PUBLICATIONS **3,311** CITATIONS
SEE PROFILE

Hong-Xing Wu
Health Canada
219 PUBLICATIONS **16,043** CITATIONS
SEE PROFILE

Environ. Sci. Technol. **2010,** *44,* 8190–8195

In-Situ Measurements of Engineered Nanoporous Particle Transport in Saturated Porous Media

JIANYING SHANG, CHONGXUAN LIU,* ZHEMING WANG, HONG WU, KAKE ZHU, JUAN LI, AND JUN LIU

Pacific Northwest National Laboratory, Richland, Washington 99354

Received May 10, 2010. Revised manuscript received August 20, 2010. Accepted September 3, 2010.

Engineered nanoporous particles have become an important class of nanostructured materials that have been increasingly applied in energy, biomedical, and environmental researches and industries. The internal pore surfaces in the particles can be chemically functionalized for environmental applications to sequestrate metals and radionuclide contaminants from groundwater. The fate and transport of the nanoporous particles in subsurface environments, however, have not been studied. Here we present a scanning optical fiber fluorescence profiler that can be used to in situ monitor the transport of fluorescent particles in column systems. Engineered nanoporous silicate particles (ENSPs) that were covalently bounded with fluorescence-emitting, and uranium-chelating ligands in the intraparticle pore domains were synthesized and used as an example to investigate nanoporous particle transport and to demonstrate the application of the developed in situ measurement profiler. The profiler detected an "irreversible" or slowly detached fraction of ENSPs in a sand collector even under thermodynamically unfavorable conditions for particle attachment. Further, the in situ measurement system detected the spatial variability of ENSPs transport that deviated from one-dimensional, homogeneous assumption, which is typically used to model particle transport in column systems. Generally, however, both measured and model-calculated results indicated that the transport of ENSPs was consistent with that of nonporous colloidal particles subjected to coupled reversible attachment/detachment and straining processes. The developed system can also be applied to detect other fluorescent nanostructured or colloidal particles in porous media.

Introduction

Engineered nanoporous particles have become an important class of nanostructured materials that have growing applications such as in bimolecular sensing and labeling, energy storage and fuel cell technology, environmental remediation, and protection (*1*). Engineered nanoporous silicate particles (ENSPs) are a major class of the engineered nanoporous particles that are made of silicate and contain nanosized intragrain pores. The ENSPs material has a large surface area (>500 m^2/g) and its internal pore surfaces can be covalently bonded with functional chemical ligands (*2*−*4*). The material can be specifically functionalized for selective sequestration of various aqueous radionuclides and metals from groundwater and wastewater (*2, 4*). The high ionic selectivity, large sorption site density, fast sorption kinetics, and stable silicate structure of ENSPs yield a potentially efficient material for capturing metals and radionuclides from contaminated groundwater. The fate and transport of the material in porous media, however, has not been studied, preventing the assessment in its applicability to remediate contaminants in subsurface environments.

Column systems are frequently used to study particle transport in porous media under advective conditions (*5*−*9*). In these studies, column breakthrough curves are used to infer transport processes such as particle retention and subsequent release, and to estimate transport parameters using the advection-dispersion equation (ADE). Various models of particle deposition and mobilization have been proposed based on the goodness-of-fit of the models to the measured effluent data (*10*−*15*). These models, together with other independent observations of particle transport at the pore scale (*16*−*18*) and in flow cell systems (*19*−*22*), have significantly advanced our understanding on particle transport processes such as straining, attachment and detachment at solid-water or air−water−solid interfaces.

Various noninvasive methods have been developed, mostly based on fluorescence imaging, to in situ measure particle transport in porous media. These methods allow direct observations of particle attachment/detachment processes and have provided important insights into the particle transport mechanisms in porous media (*16*−*22*). The noninvasive methods, however, have a difficulty to be applied to detect particle transport in column systems because of the difficulty in delivering lights to and/or receiving fluorescence signals from inside columns. This difficulty can be overcome by invasive methods that rely on sensors buried inside columns for deliverying and receiving lights. Such methods have been demonstrated in measuring tracer and gas phase chemical concentrations in sand columns (*23*−*25*). However, direct measurements of particle transport inside columns have not been reported to our knowledge. These in situ measurements are important to validate the one-dimensional homogeneous assumption often used in deriving ADE models with assumed particle transport processes in column systems, and may further advance our knowledge in particle transport within porous media.

Here we report a scanning optical fiber fluorescence profiler that was developed to in situ track ENSPs transport within a sand column. The internal pore surfaces of the synthesized ENSPs were covalently bonded with fluorescence-emitting functional ligands, which were monitored as a function of time and distance in the column under a saturated flow condition. The ENSPs and sand surface properties were independently measured to provide insights into the interactions between ENSPs and sand collector. Nitrate was used as a tracer to probe the dispersion property. The measured fluorescence signals emitted from ENSPs were used to calculate the total (aqueous + attached) ENSPs concentrations inside the column, which were used to validate particle transport models estimated from the effluent data.

Materials and Methods

ENSPs. Functionalized ENSPs were synthesized following a procedure described elsewhere (*3*). The procedure was modified specifically for this study to generate particles with a desired particle size (~300 nm), intragrain pore diameter (~5 nm), and surface chemistry (ref *26*, also see Supporting Information (SI)). The internal pore surfaces of the ENSPs

* Corresponding author phone: (509)371-6350; fax (509)371-6354; e-mail: Chongxuan.Liu@pnl.gov.

10.1021/es1015586
Published on Web 10/01/2010

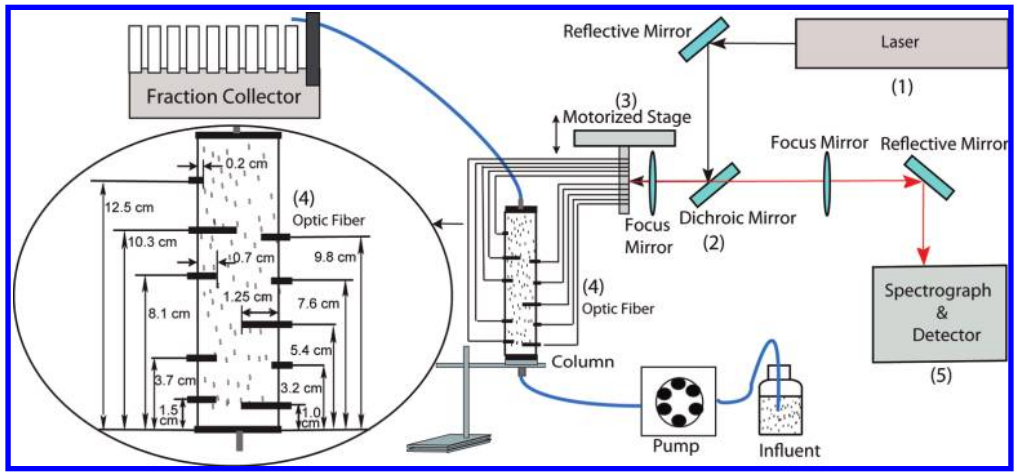

FIGURE 1. Schematic diagram showing the scanning optical fiber fluorescence profiler and the spatial distribution of optical fibers in the column used to measure ENSPs transport. Corresponding photos of the profiler were provided in Figures S1 and S2 in SI.

were covalently bonded with a monolayer of salicylamide ligands, which can produce fluorescence signals for in situ particle tracking and also chelate contaminant uranium from aqueous solutions. The later property is important for ENSPs applications in sequestrating contaminants from groundwater (*2, 4, 27*). The measured dry and wet densities of ENSPs were 0.971 and 1.335 g/cm^3, yielding an intragrain porosity of 36.4%. The hydrodynamic particle size and electrophoretic mobility of the ENSPs were measured by dynamic light scattering (DLS) using a Zetasizer 3000HAS (Malvern Instruments Ltd., Malvern, UK). The particle morphology was determined by transmission electron microscope (TEM, JEOL JEM-2010 TEM).

Transport Experiments. Column experiments were conducted in a stainless steel column (2.5 cm i.d. and 15 cm length). The bottom and top of the column were equipped with a porous steel screen (50 μm pore diameter). Influent solution was applied upward into the column at a desired flow rate using a high performance HPLC pump. The column was wet-packed to avoid air entrapment. Quartz sand (Accusand 40/60) was used as the particle collector with a size ranging from 300 to 355 μm. The sand was pretreated with 0.25 M NaOH and 0.25 M HCl to remove impurity, and then repeatedly rinsed with deionized water until pH stabilized. The treated sand was air-dried and then used for surface characterization and column experiments. The average bulk density of the packed column was 1.66 g/cm^3 with a porosity of 0.38.

Synthetic groundwater (SGW) with the same chemical composition as that in groundwater at the U.S. Department of Energy's Hanford site (pH 8.1 and ionic strength 6.3 mM) (*28*) was used as a background solution. The SGW was spiked with nitrate (3 mM) to probe the hydrodynamic dispersion in the column. Before injecting ENSPs, the ENSPs-free SGW was introduced into the column for at least five pore volumes (PVs) to chemically equilibrate the solids with the SGW. The ENSPs-containing SGW was prepared by mixing ENSPs with SGW at a particle concentration of 0.15 g/L (1.01×10^{13} particles/L), sonicated for half an hour to disperse the particles, and then stored in the column injection solution reservoir. The reservoir solution was continuously stirred with a magnetic bar to maintain ENSPs dispersion. The effluents from the column were collected for measurements by a programmed fraction collector. Nitrate and ENSPs concentrations in the effluents were measured using a UV−vis spectrophotometry (UV-2501 PC, Shimadzu Scientific Instruments, Columbia, MD) at a wavelength of 235 and 301 nm, respectively.

Scanning Optical Fiber Fluorescence Profiler (SOFFP). The SOFFP consists of five major components: light source, mirror system, motorized stage, optical fibers, and detector (Figure 1, and Figures S1 and S2 in SI). A helium cadmium laser (74 omnichrome, Garlsbad, CA) with an emission wavelength of 325 nm was used as the excitation light source. The laser beam was reflected by a dichroic mirror and focused into the optical fibers. The dichroic mirror is reflective if the light wavelength is shorter than 350 nm and becomes transparent if wavelength above 350 nm. The optical fibers (1 mm diameter) (PCU-1000−1, Multimode Fiber Optics Inc., Hackettstown, NJ) were mounted on a motorized stage, which was programmed to align individual fibers to the focused light source at predefined time intervals. The other end of the fiber was inserted into the column directly across the column wall using flangeless chromatography fitting to deliver the excitation laser lights and collect fluorescence emission. The collected fluorescence passed through the dichroic mirrors, dispersed by a spectrograph (SpectraPro 150, Acton Research Corporation, Acton, MA), and detected by an intensified CCD detector (PIMAX, Roper Scientific). There were ten optical fibers with their tips located at 1.0, 1.5, 3.2, 3.7, 5.4, 7.6, 8.1, 9.8, 10.3, and 12.5 cm from the column inlet (Figure 1). The distances of the fiber tips from the column wall were also varied: three tips were at the centers (12 mm from the wall), four at the half radius (7 mm), and three near (2 mm from) the wall to investigate the spatial variability of particle transport.

Calibration. The measured fluorescence intensity linearly correlated with the ENSPs concentration at different optical fiber locations in the column containing ENSPs suspensions (Figure S3 in SI). The variation of the calibration curves at the different fiber locations was attributed to the difference of the optical fiber properties such as tip diameter, surface roughness, and light transmission because sand was not provided in the column. Direct calibration to determine the correlation between ENSPs concentration and fluorescence intensity in the sand column was not possible under our experimental conditions because of the difficulty to know the ENSPs concentrations at specific fiber locations. Such concentrations were affected by local pore structure such as pore to solid volume ratio and particle transport properties that affect spatiotemporal attachment/detachment along flow paths.

To provide insights into the influence of sand porous media on ENSPs measurements, two additional calibration experiments were performed in batch systems. The first experiment was to determine the laser light attenuation and penetration in the sand porous media with the same macroscopic property (i.e., saturated sand with a porosity = 0.38) as in the column for the ENSPs transport experiments. Figure S4a in SI showed that over 99% of excitation laser light was

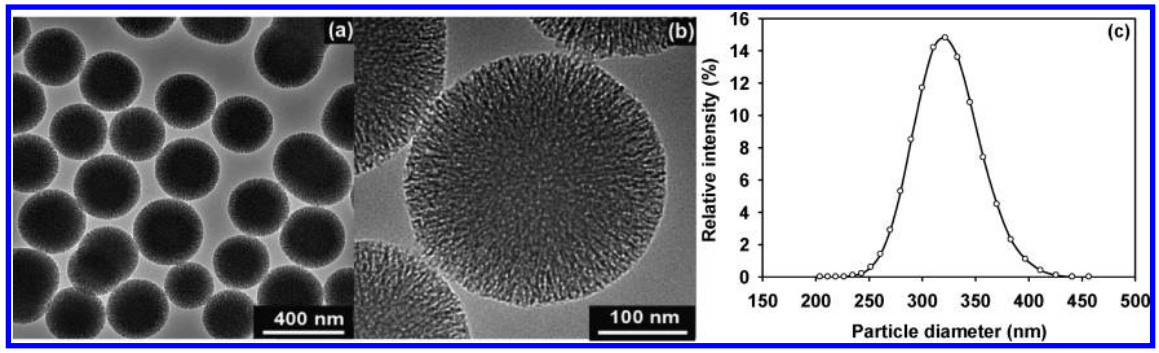

FIGURE 2. Transmission electron micrographs (plots a and b) and particle size distribution of ENSPs (plot c).

attenuated after 1 mm penetration in the porous media. The result indicated that the fluorescence signals collected by each optical fiber were from a cylindrical volume (~0.8 mm^3) in front of the fiber tip with a diameter of 1 mm and a length of 1 mm. The second calibration experiment was to determine the linear correlation between the fluorescence signal intensity and ENSPs concentration in saturated sand porous media in the batch setup (Figure S4b in SI). The results in Figure S4b were derived by first wet-mixing sand with ENSPs in batch systems and then the mixed material was packed in a cuvette (1 × 1 × 4 cm) with the same solid/water ratio (i.e., porosity = 0.38) as used for the column experiment. The calibration curve (Figure S4b in SI) determined from the batch system cannot be directly applied to each fiber inside the column because of the effects of fiber material variations (Figure S3 in SI). To overcome this difficulty, for each calibration curve in Figure S3 and Figure S4b, we normalized the measured fluorescence intensity values to a fluorescence intensity corresponding to a reference ENSPs concentration (e.g., 0.12 g/L). After this normalization procedure, all the calibration curves (Figure S3 and Figure S4b) collapsed to form one curve because of their linearity. Finding the reference ENSPs concentration and applying the normalized calibration curve to determine ENSPs concentration were discussed in the next section.

Results and Discussion

ENSPs Properties. TEM analysis revealed the spherical shape of the ENSPs with a comb-type pore structure in the intragrain region and a nominal internal pore diameter of 5 nm (Figure 2a and b). The particle size followed a normal distribution ranging from 200 to 450 nm with a mean size of 308 nm and a standard deviation of 15 nm (Figure 2c).

The aggregation of ENSPs and stability of surface-bound salicylamide ligands are two important properties that will affect the transport and detection of ENSPs during the experiments. The detail synthesis procedure for deriving desired ENSPs was described elsewhere (*26*). Briefly, various types of salicylamide-coated ENSPs were synthesized by varying temperature, surfactant types, ligand bonding procedures, and postsynthesis treatment that produced the materials with variable properties in aggregation and stability of salicylamide ligands. The ENSPs material with the minimal aggregation property and best stability of surface-bound ligands under the column experimental conditions was selected to minimize the complexity of data interpretation. The experimental conditions used in generating the ENSPs for this study were provided in SI. Measurements pre- and during the column experiments all confirmed that surface-coated salicylamide ligands in the selected material were stable during the entire experiments. Measurements also confirmed that ENSPs had a consistent size distribution and zeta potential in the influent and selected effluent samples from the column. Independent batch studies found that the dispersed ENSPs were stable in the column injection solution reservoir under stirred conditions.

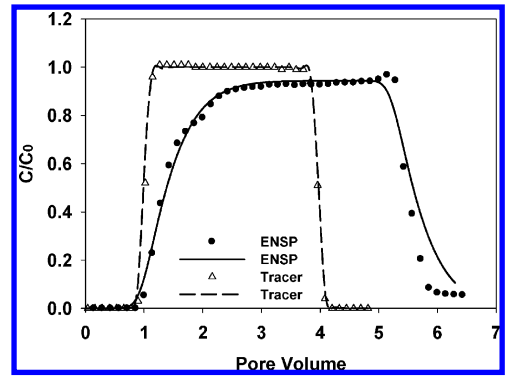

FIGURE 3. Measured (symbols) and model-calculated (lines) effluent breakthrough curves of tracer and ENSPs. *C* and C_0 are the aqueous concentrations of either tracer or ENSPs in the effluent and influent solutions, respectively.

DLVO Interactions. The measured zeta potentials of ENSPs and sand collector in the SGW were −19.0 and −27.5 mV, respectively. The measured zeta potentials in the SGW were used to calculate the interaction energies between particles and sands based on the Derjaguin−Landau−Verwey−Overbeek (DVLO) theory. The detail calculation procedure and results were provided in SI section 4 and Figure S5. Briefly, the calculations found a primary high energy barrier (~ 100 *k*T) near 1 nm and secondary low energy minimum (−0.17 *k*T) at 30.5 nm from the sand surface. These energy values indicated that the ENSPs attachment to the sand collector was thermodynamically unfavorable under our experimental conditions (*7*).

Effluent Tracer and ENSPs. The breakthrough curve of the nonreactive tracer (NO_3^-) in the sand column was symmetric (Figure 3), indicating that the tracer transport was ideal, consistent with the advection and dispersion model. This was expected because of the homogeneous packing of the quartz sands in the column. The effluent ENSPs were detected starting at 0.8 pore volume (PV), then its concentration (C/C_0, C_0 is the ENSPs in the injection solution) rapidly increased to 0.8 near the second PV, followed by a slow increase toward a plateau concentration ($C/C_0 = 0.95$) at the third PV. The deviation between the tracer and ENSPs effluent profiles was attributed to the deposition of the ENSPs in the column despite the unfavorable attachment condition based on the calculated DLVO interaction energies. Mass balance calculation between the influent and effluent ENSPs concentrations revealed that 37−40% of particles in the column were attached to the solids after 3−4 PV of particle injection. The particle attachment under unfavorable conditions was reported previously and was attributed to the effect of the secondary energy minimum (*7*, *29*−*32*).

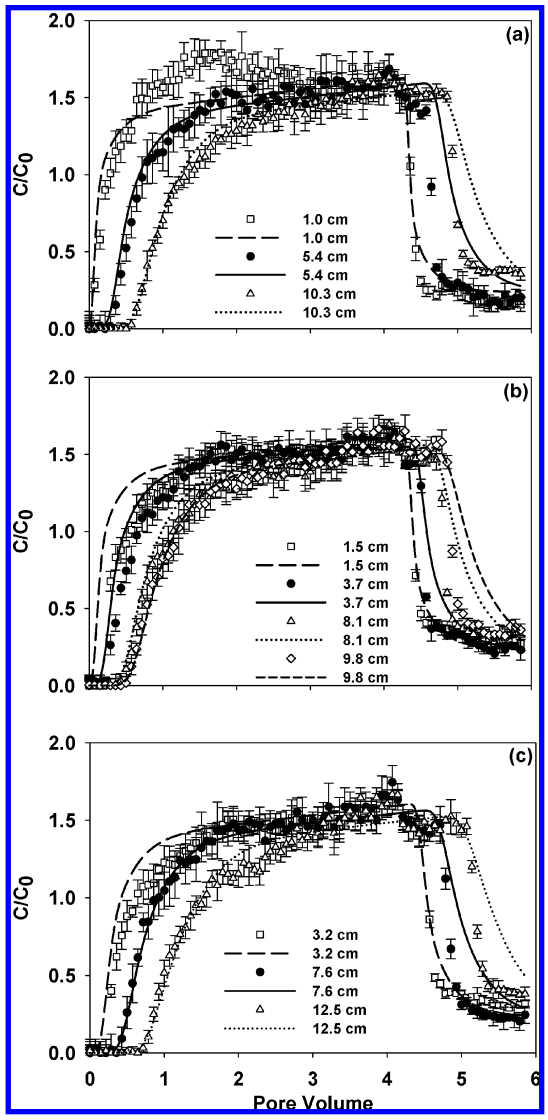

FIGURE 4. Normalized ENSPs concentrations as a function of time at various locations inside the column (*C* is the total (aqueous + attached) concentration and C_0 is the aqueous concentration in the influent solution). Plot a showed the results at three locations in the center of column (12 mm from the column wall); plot b showed the results at four half radius locations (7 mm from the column wall); and plot c showed results at three locations near (2 mm from) the column wall. Symbols were estimated from the measured fluorescence intensity values, and lines were model-calculated. The distance from each optical fiber to the column inlet was provided in the plot legends. The error bar represented one standard deviation of four replicate measurements.

After injection of ENSPs-free SGW at 4.3 PV, the effluent ENSPs concentration maintained at the plateau concentration for about 1 PV (Figure 3), then quickly decreased to 0.05 (C/C_0). Mass balance calculations showed that over 90% of the previously attached particles were removed after 2 PV injection of ENSPs-free SGW, consistent with the prediction from the calculated DLVO energies that most attached particles during the injection step were unstable at the secondary energy minimum. The tailing of the ENSPs concentration ($C/C_0 = 0.05$) after the sixth PV indicated that a fraction of the attached ENSPs was controlled by the rate-limited detachment process.

In Situ Concentration Profiles from Optical Fibers. The ENSPs concentrations inside the column changed significantly as a function of time and spatial location (Figure 4).

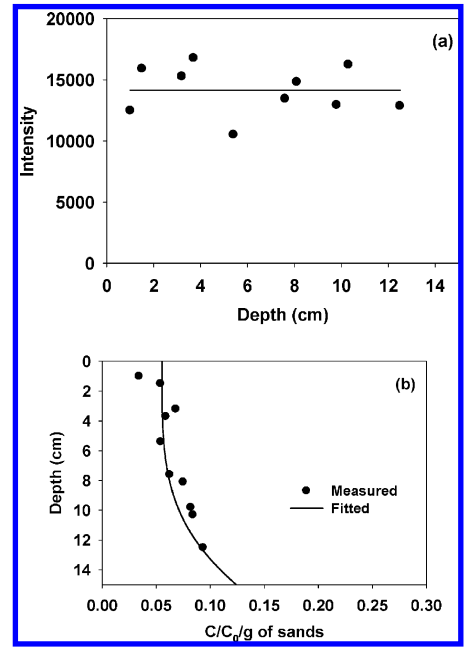

FIGURE 5. Measured fluorescence intensity values as a function of spatial distance from the column inlet after 4 PV of ENSPs injection (plot a) and residual ENSPs concentrations as a function of distance after 2 PV of ENSPs-free SGW injection (plot b).

The reported concentrations included aqueous and attached ENSPs that emitted the fluorescence signals. In Figure 4, the particle concentration and error bar represented the averaged concentration and one standard deviation, respectively, from four replicate measurements. The particle concentration at a specific location was calculated from the normalized fluorescence intensity as a function of time. As discussed in the calibration section, the measured fluorescence intensity was affected by optical fiber properties and local pore structure that affected light delivery and collection. Figure 5a showed the variable measured fluorescence intensity values at different fiber locations after 4 PV injections of ENSPs. The calculated variability (one standard deviation) was 14% of the averaged fluorescence intensity value (Figure 5a solid line). Such variation was difficult to eliminate by adjusting the column packing procedure because of the uncertainties in controlling the local pore structures. To minimize such local pore structure effect, the measured fluorescence intensity was normalized to the local fluorescence intensity at PV 4 when the fluorescence intensity was near the "steady state" at each monitoring location, and effluent particle concentration was at the plateau value (Figure 3) before the particle-free solution was injected. This normalization procedure also eliminated the effects of fiber material variations on the fluorescence measurements (Figure S3 in SI) as discussed in the calibration section. Mass balance calculations between the influent and effluent ENSPs concentrations indicated that the averaged total particle concentration in the column was 158% of the influent concentration after four pore volumes of particle injection. This concentration ratio (1.58) was then used as the reference ENSPs concentration for the normalized calibration curve as discussed in the calibration section. The ENSPs concentration was determined from the normalized calibration curve based on the measured and normalized fluorescence signal intensity at each fiber location.

The estimated particle concentrations at different optical fibers showed similar trends except at the first fiber (at 1 cm from the column inlet) (Figure 4). After breakthrough, the concentration ratio (C/C_0, where C is the total (aqueous +

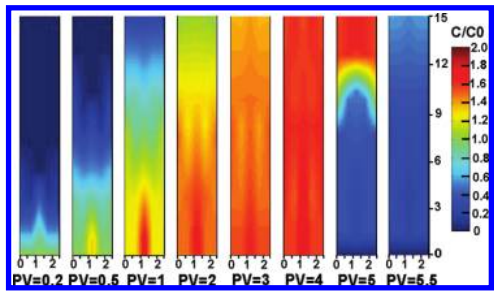

FIGURE 6. Two dimensional (longitudinal and radial) distributions of normalized ENSPs concentration (C/C_0) as a function of time. The plots were interpolated from the results in Figure 4.

attached) ENSPs concentration and C_0 is the aqueous concentration in the influent solution) increased rapidly to 1.4 with time, and then slowly approached to the steady state value 1.58. The higher concentration ratio than 1.58 at the first fiber may have resulted from the preferential accumulation of the particles near the column inlet as reported in other studies (*10, 12, 32, 33*). When the ENSPs-free SGW was injected, the particle concentration decreased quickly until they arrived at the "tailing" plateau. The tails of the ENSPs concentration profiles inside the column were similar to, but higher than that in the effluent (Figure 3). The tail concentrations changed slowly with time at all the monitoring locations, consistent with the inference from the effluent data that a fraction of attached particles detached slowly. Such slowly detaching particles were most likely associated with the primary attachment minimum with a high energy barrier (Figure S5, SI), or at the solid−solid contact domains by a straining process (*13, 33*). The tail concentrations generally increased from the column inlet toward the outlet (Figure 5b), consistent with the advective removal of the attached particles.

Two dimensional interpolations of the particle concentrations inside the column showed that the ENSPs transport was generally consistent with one-dimensional advective transport as a function of time (Figure 6). However, the results also showed a relatively faster rate of particle transport in the column center. The particle removal by the ENSPs-free SGW solution was also faster at fibers closer to the center line, suggesting that the faster particle transport along the column center line was likely caused by the faster fluid flow that carried particle transport despite the fact that the nonreactive tracer showed an ideal transport behavior (Figure 3). It was unclear, however, whether such a faster flow in the column center was a general phenomenon or specifically caused by the column design. Further researches are needed to resolve this problem, which is important for characterizing particle attachment/detachment processes using column systems.

Modeling. The ENSP particle concentrations in the effluent (Figure 3) and in the column at the end of the experiment (Figure 5b) were collectively used to determine the parameters in the particle attachment and detachment models (Eqs S3 and S4 in SI). Simultaneously using the effluent data and particle concentrations inside the column at the end of experiments has been shown to provide a better estimation of model parameters than using the effluent data only (*10*). The fast removal of a large fraction of the attached particles after the injection of the ENSPs-free SGW, and a consistent tailing at all monitoring locations (Figure 4) and in the effluent (Figure 3) suggested that there were two pools of particle attachment sites: fast or reversible pool and slow detaching or straining pool. Here the reversible site was modeled using a first-order model with an attachment constant k_{att}, and detachment constant k_{det} (eq S3 in SI) (*10, 15, 34*) and straining was modeled using an irreversible first-order model with a rate constant k_{irr} (eq S4 in SI) (*15, 34*). The best fit between the calculated and observed data (Figures 3 and 5b) yielded parameter values of 0.4, 1.0, and 0.012 h^{-1} for k_{att}, k_{det}, and k_{irr}, respectively. The estimated k_{att} and k_{det} were much larger than k_{irr}, indicating that the reversible process dominated overall particle attachment-detachment processes. The small, nonzero value of k_{irr} implied the existence of the irreversible deposition process. These results were consistent with the mass balance calculations based on the effluent and in situ measured results that 90% of the attached particles were removed with the 2 PV injections of the ENSPs-free SGW.

The particle transport model with fitted parameters was then used to predict the particle concentration changes as a function of time inside the column (lines in Figure 4). Generally the predicted values matched well with the monitored particle concentrations at the fiber tips (Figure 4). The model, however, underestimated the particle concentrations from 0.5 to 3 PV at the distance 1 cm, but overestimated particle concentrations from 0.5 to 2 PV at the distance 1.5 to 3.7 cm. These discrepancies supported that the particles were preferentially accumulated near the column inlet (1 cm) (*10−12, 32−34*), and this preferential attachment decreased particle concentrations at the immediate downgradient locations (1.5−3.7 cm). Such preferential attachment was not considered in the model. The particle concentrations at 1 cm location decreased to the predicted value after 3 PV, indicating that the early attached particles were partially released. The reason for this decrease was unclear and cannot be explained based on current particle transport models.

Implication. The increasing application of engineered nanoporous particles (ENPs) in various industries and research areas has raised environmental concerns on their fate and transport in air, water, and subsurface environments. Our results implied that the transport of ENPs will be generally similar as the nonporous colloidal particles because of their similar surface energetic properties. The current attachment and detachment models of nonporous particles can be used to approximately describe the ENPs transport in porous media. A scanning optical fiber fluorescence profiler was developed, which can be used to provide additional data (e.g., Figures 4 and 5) besides the effluents for understanding the mechanisms controlling particle transport and validating transport processes that occur inside the column. The developed system is particularly useful for directly studying the fate and transport of nanoporous particles without using particle surrogates because the internal pores of the particles can be tagged with fluorescent chemical compounds without affecting the particle surface properties, which primarily control particle transport. In addition, the developed in situ fluorescence measurement system may be extended to a large scale to evaluate particle transport in physical heterogeneous system.

The developed profiler belongs to a type of invasive in situ measurement approaches that are typically difficult to in situ calibrate the probers or sensors in uncontrolled local porous media, especially for those sorbing chemicals that would be strongly affected by local surface area to pore volume ratios. In this study, a normalized fluorescence intensity approach was used to overcome this difficulty. The normalization procedure also eliminated the effects of potential fiber material variations at different monitoring locations. The invasive approach may also suffer the interference of the buried sensors and fibers into fluid flow and particle transport. In the current case, the small size (1 mm in diameter) of the optical fibers and tips reduced the invasive influence on the interior structure of the porous media.

Acknowledgments

This research was supported by U.S. Department of Energy (DOE) Office of Biological & Environmental Research (BER) through a joint EPA-NSF-DOE research program. The Research was performed at Environmental Molecular Science Laboratory (EMSL), a DOE national user facility located at Pacific Northwest National Laboratory (PNNL). PNNL is operated by Battelle Memorial Institute under subcontract DE-AC06-76RLO 1830.

Supporting Information Available

Synthesis of ENSPs, photographs of scanning optical fiber fluorescence profiler, calibration curves, DLVO Interaction energy and force Profiles, mathematical models. This material is available free of charge via the Internet at http://pubs.acs.org.

Literature Cited

(1) Lu, G. Q.; Zhao, X. S. *Nanoporous Materials: Science and Engineering*; Imperial College Press: London, 2004.
(2) Feng, X.; Fryxell, G. E.; Wang, L.-Q.; Kim, A. Y.; Liu, J.; Kemner, K. M. Functionalized monolayers on ordered mesoporous supports. *Science* **1997**, *276* (5314), 923–926.
(3) Liu, J.; Feng, X.; Fryxell, G. E.; Wang, L.-Q.; Kim, A. Y.; Gong, M. Hybrid mesoporous materials with functionalized monolayers. *Adv. Mater.* **1998**, *10* (2), 161–165.
(4) Fryxell, G. E.; Liu, J.; Hauser, T. A.; Nie, Z.; Ferris, K. F.; Mattigod, S.; Gong, M.; Hallen, R. T. Design and synthesis of selective mesoporous anion traps. *Chem. Mater.* **1999**, *11*, 2148–2154.
(5) Bradford, S. A.; Bettahar, M.; Simunek, J.; van Genuchten, M. T. Straining and attachment of colloids in physically heterogeneous porous media. *Vadose Zone J.* **2004**, *3* (2), 384–394.
(6) Torkzaban, S.; Tazehkand, S. S.; Walker, S. L.; Bradford, S. A. Transport and fate of bacteria in porous media: coupled effects of chemical conditions and pore space geometry. *Water Resour. Res.* **2008**, *44*, W04403, DOI: 10.1029/2007WR006541.
(7) Shen, C. Y.; Li, B. G.; Huang, Y. F.; Jin, Y. Kinetics of coupled primary- and secondary-minimum deposition of colloids under unfavorable chemical conditions. *Environ. Sci. Technol.* **2007**, *41* (20), 6976–6982.
(8) Zhuang, J.; Jin, Y.; Flury, M. Comparison of Hanford colloids and kaolinite transport in porous media. *Vadose Zone J.* **2004**, *3* (2), 395–402.
(9) Lenhart, J. J.; Saiers, J. E. Colloid mobilization in water-saturated porous media under transient chemical conditions. *Environ. Sci. Technol.* **2003**, *37* (12), 2780–2787.
(10) Bradford, S. A.; Simunek, J.; Bettahar, M.; Van Genuchten, M. T.; Yates, S. R. Modeling colloid attachment, straining, and exclusion in saturated porous media. *Environ. Sci. Technol.* **2003**, *37* (10), 2242–2250.
(11) Bradford, S. A.; Bettahar, M. Straining, attachment, and detachment of Cryptosporidium oocysts in saturated porous media. *J. Environ. Qual.* **2005**, *34* (2), 469–478.
(12) Bradford, S. A.; Bettahar, M. Concentration dependent transport of colloids in saturated porous media. *J. Contam. Hydrol.* **2006**, *82* (1−2), 99–117.
(13) Xu, S. P.; Gao, B.; Saiers, J. E. Straining of colloidal particles in saturated porous media. *Water Resour. Res.* **2006**, *42*, W12S216, DOI: 10.1029/2006WR004948.
(14) Xu, S. P.; Liao, Q.; Saiers, J. E. Straining of nonspherical colloids in saturated porous media. *Environ. Sci. Technol.* **2008**, *42* (3), 771–778.
(15) Hendry, M. J.; Lawrence, J. R.; Maloszewski, P. The role of sorption in the transport of *Klebsiella oxytoca* through saturated silica sand. *Ground Water* **1997**, *35* (4), 574–584.
(16) Gao, B.; Saiers, J. E.; Ryan, J. Pore-scale mechanisms of colloid deposition and mobilization during steady and transient flow through unsaturated granular media. *Water Resour. Res.* **2006**, *42*, W01410, DOI: 10.1029/2005WR004233.
(17) Bradford, S. A.; Kim, H. N.; Haznedaroglu, B. Z.; Torkzaban, S.; Walker, S. L. Coupled factors Influencing concentration-dependent colloid transport and retention in saturated porous media. *Environ. Sci. Technol.* **2009**, *43* (18), 6996–7002.
(18) Wan, J. M.; Wilson, J. L. Visualization of the role of the gas-water interface on the fate and transport of colloids in porous-media. *Water Resour. Res.* **1994**, *30* (1), 11–23.
(19) Zhang, P. F.; Wang, Y. G. Epi-fluorescence imaging of colloid transport in porous media at decimeter scales. *Environ. Sci. Technol.* **2006**, *40* (19), 6064–6069.
(20) Bridge, J. W.; Banwart, S. A.; Heathwaite, A. L. Noninvasive quantitative measurement of colloid transport in mesoscale porous media using time lapse fluorescence imaging. *Environ. Sci. Technol.* **2006**, *40* (19), 5930–5936.
(21) Bridge, J. W.; Banwart, S. A.; Heathwaite, A. L. High-resolution measurement of pore saturation and colloid removal efficiency in quartz sand using fluorescence imaging. *Environ. Sci. Technol.* **2007**, *41* (24), 8288–8294.
(22) Bridge, J. W.; Heathwaite, A. L.; Banwart, S. A. Measurement of colloid mobilization and redeposition during drainage in quartz sand. *Environ. Sci. Technol.* **2009**, *43* (15), 5769–5775.
(23) Treadaway, A. C. J.; Lynch, R. J.; Bolton, M. D. Pollution transport studies using an in-situ fibre optic photometric sensor. *Eng. Geol.* **1999**, *53* (2), 195–204.
(24) Jung, H.; Choi, H.; Kim, J.; Schwartz, F. W. Laboratory-scale application of fiber optic transflection dip probe (FOTDP) for in situ monitoring of gas phase ozone in unsaturated porous media. *J. Contam. Hydrol.* **2006**, *82* (1−2), 133–144.
(25) Huang, W. E.; Smith, C. C.; Lerner, D. N.; Thornton, S. F.; Oram, A. Physical modelling of solute transport in porous media: Evaluation of an imaging technique using UV excited fluorescent dye. *Water Res.* **2002**, *36* (7), 1843–1853.
(26) Li, J.; Zhu, K. K.; Shang, J. Y.; Wang, D. H.; Nie, Z. M.; Guo, R. S.; Liu, C. X.; Wang, Z. M.; Li, X. L.; Liu, J. *Fluorescent Functionalized Mesoporous Silica for Radioactive Material Extraction. J. Nanomater.* (submitted).
(27) Liu, C.; Zachara, J. M.; Smith, A. C.; McKinley, J. P.; Answorth, C. C. Desorption kinetics of radiocesium from subsurface sediments at Hanford Site, USA. *Geochim. Cosmochim. Acta* **2003**, *67* (16), 2893–2912.
(28) Liu, C.; Zachara, J. M.; Qafoku N. P.; and Wang, Z. Scale-dependent desorption of uranium from contaminated subsurface sediments. *Water Resour. Res.* **2008**, *44*, DOI: 10.1029/2007WR006478.
(29) Tufenkji, N.; Elimelech, M. Deviation from the classical colloid filtration theory in the presence of repulsive DLVO interactions. *Langmuir* **2004**, *20* (25), 10818–10828.
(30) Tufenkji, N.; Elimelech, M. Breakdown of colloid filtration theory: Role of the secondary energy minimum and surface charge heterogeneities. *Langmuir* **2005**, *21* (3), 841–852.
(31) Hahn, M. W.; O'Melia, C. R. Deposition and reentrainment of Brownian particles in porous media under unfavorable chemical conditions: Some concepts and applications. *Environ. Sci. Technol.* **2004**, *38* (1), 210–220.
(32) Hahn, M. W.; Abadzic, D.; O'Melia, C. R. Aquasols: On the role of secondary minima. *Environ. Sci. Technol.* **2004**, *38* (22), 5915–5924.
(33) Bradford, S. A.; Simunek, J.; Bettahar, M.; van Genuchten, M. T.; Yates, S. R. Significance of straining in colloid deposition: Evidence and implications. *Water Resour. Res.* **2006**, *42*, W12S15, DOI: 10.1029/2005WR004791.
(34) Yoon, J. S.; Germaine, J. T.; Culligan, P. J. Visualization of particle behavior within porous medium: Mechanisms for particle filtration and retardation during downward transport. *Water Resour. Res.* **2006**, *42*, W06417, DOI: 10.1029/2004WR003660.

ES1015586